RSC Advances

PAPER

View Article Online
View Journal | View Issue

Cite this: *RSC Adv.*, 2017, **7**, 40255

Synthesis of optically tunable bumpy silver nanoshells by changing the silica core size and their SERS activities†

Hyejin Chang,‡[a] Eunbyeol Ko,‡[a] Homan Kang,§[b] Myeong Geun Cha,[a] Yoon-Sik Lee*[b] and Dae Hong Jeong *[a]

The fabrication of hollow metal nanostructures on a silica core template has been widely studied by taking advantage of the chemical stabilities of silica cores. When the size of the silica core reduces, however, this benefit is no longer effective because there are the synthetic difficulties which often cause dispersion instability, and therefore finally the aggregations of nanoparticles (NPs) are often caused during introduction of metallic nanostructures. This study reports the successful fabrication of silver nanoshells (AgNSs; 119, 152, 165, 186, and 207 nm) on amorphous silica nanoparticles (Si NPs) of different core sizes (59, 82, 103, 124, and 148 nm) by overcoming the increased instabilities during fabrication with reduced core sizes. Improvements related to fabrication were made by changing the reducing agents, controlling the amount of the dispersing agent and the concentration of Si NPs. All the AgNSs showed broad extinction from the visible to the near-infrared (NIR) region regardless of particle sizes, and their size-dependent surface properties were analyzed by introducing a concept of roughness factor, with AgNS of 152 nm exhibiting the highest degree of roughness. High SERS enhancements of AgNSs of all sizes were observed at three laser excitation wavelengths (532, 660, and 785 nm), and these enhancements correlated positively with the surface roughness. Therefore, our results provide a clear understanding of size-dependent SERS activity for AgNS, facilitating proper selection of AgNS with an appropriate size depending on the purpose of the investigation.

Received 2nd June 2017
Accepted 7th August 2017

DOI: 10.1039/c7ra06170f

rsc.li/rsc-advances

Introduction

Surface-enhanced Raman scattering (SERS) has been extensively studied in various fields such as material science,[1,2] physical chemistry[3] and nanobiotechnology due to its outstanding sensitivity affording single-molecular level detection,[2,4] multiplexing capability and resistance to photobleaching.[5] For optical tuning of localized surface plasmon resonance (LSPR), several classes of metal nanoparticles (NPs) such as nanoshells,[6–8] hollow nanospheres,[9] nanorods,[10] and nanostars,[11] have been developed as promising SERS substrates. Of these substrates, nanoshells consisting of silica cores surrounded by noble metals, usually gold or silver, can be controlled to have unique optical properties. For example, LSPR bands can be tuned from the visible to the near-infrared (NIR) region by changing shell thicknesses and core size.[12–16] This optical tunability contributes to biosensing and imaging applications of nanoshells as SERS-active substrates.[14,15,17] However, with respect to their synthesis, fabricating a metal shell on a small-sized silica core (<100 nm) is problematic because of aggregation of the hybrid structures. The NPs tend to decrease their surface energies during synthesis. In addition, the NPs with smaller core sizes and high surface curvatures have higher critical energy barriers (ΔG^*) resulting in incomplete and non-uniform metal shells.[6] Hence, the deposition of a uniform and complete metal shell on a smaller core still remains a challenge.[18]

Metal nanoshells have been developed by several synthetic routes such as seed-mediated growth,[5,6,11,12] multistep layer-by-layer (LBL) deposition,[13,14] thermal evaporation methods,[15] and sonochemical processes.[16] Recently, our group has reported on a simple and one step seedless fabrication method for bumpy silver nanoshells (AgNSs). They are effective in SERS enhancement compared to a smooth metal shell owing to the high concentration of the electromagnetic field at the rough

[a]*Department of Chemistry Education, Seoul National University, Seoul 08826, Republic of Korea. E-mail: jeongdh@snu.ac.kr*

[b]*Interdisciplinary Program in Nano-Science and Technology and School of Chemical and Biological Engineering, Seoul National University, Seoul 08826, Republic of Korea. E-mail: yslee@snu.ac.kr*

† Electronic supplementary information (ESI) available: Tables of synthetic conditions and details, analysis of AgNSs of size distributions and SERS properties, optimization processes and other materials are included in the ESI. See DOI: 10.1039/c7ra06170f

‡ These authors contributed equally to this work.

§ Present address: Department of Radiology, Harvard Medical School and Gordon Center for Medical Imaging, Massachusetts General Hospital, Boston, Massachusetts 02114, United States.

bumpy surfaces.[19–21] During the process, Ag^+ ions are reduced by alkylamine through single electron transfer from the amino group of alkylamine to the Ag^+ ions under mild conditions (room temperature), and then Ag^0 atoms are nucleated to form a Ag shell.[8,21] This facile reduction of Ag^+ ions is ascribed to a significant increase in their reduction potentials in ethylene glycol.[20,21] The increase in their reduction potentials allows the favourable electron transfer, even from the amino group to the Ag^+ ions at room temperature.

Here, we report on the size-dependent optical characteristics of AgNSs by extending our previous studies. We controlled the sizes of AgNSs by changing the sizes of the silica cores ranging from *ca*. 60 to 150 nm. Consecutive LSPR and SERS profiles were explored for AgNSs with different sizes. By varying the sizes of AgNSs, the peaks of the surface plasmon absorption bands could be tuned, while all the AgNSs exhibited broad extinction bands over the range of 350–800 nm regardless of each particle size. The roughness of AgNSs was defined and calculated, affording an insight into the size-dependent SERS activities with high enhancement factors under three different laser excitation wavelengths (532, 660, and 785 nm).

Materials and methods

Materials

Tetraethyl orthosilicate (TEOS), Triton X-100 (for molecular biology), cyclohexane (anhydrous, 99.5%), 1-hexanol (reagent grade, 98%), 3-mercaptopropyltrimethoxysilane (MPTS), ethylene glycol (spectrophotometric grade, ≥99%), silver nitrate ($AgNO_3$, 99.99%), polyvinylpyrrolidone (PVP, average M.W. 40 000), ammonium hydroxide (NH_4OH, 28–30%), octylamine, ethanolamine, and 4-fluorobenzenethiol (4-FBT) were obtained from Sigma-Aldrich (St. Louis, MO, USA). Absolute ethanol (99.9%) and anhydrous ethanol (99%) were purchased from Daejung (Busan, Korea). All chemicals were used without further purification.

Synthesis of silica core nanoparticles of different size

The silica nanoparticles (Si NPs) of *ca.* 100 nm diameter or less were synthesized by a reverse micelle method.[22] To vary the size of Si NP, we controlled the concentrations of Triton-X as a surfactant, 1-hexanol as a co-surfactant, and ammonium hydroxide. The detailed conditions used are summarized in ESI Table S1.† Triton-X, and 1-hexanol were dissolved in 7.7 mL of cyclohexane, and 350 μL of deionized water. The resulting mixture was stirred at 700 rpm for 10 min. After the reverse micelles were formed in oil phase, aqueous ammonium hydroxide (28–30%) and 50 μL of TEOS were added to the mixture. The reaction was continued for 20 h while the mixture was vigorously stirred at room temperature. The synthesized Si NPs were centrifuged and then washed with ethanol several times to remove excess reagents. The sizes of Si NPs obtained were estimated to have diameters of 42, 59, 82, and 103 nm respectively. The Si NPs that are larger than 100 nm were synthesized by the Stöber method.[23] A 1.6 mL aliquot of TEOS was dissolved in 40 mL of absolute ethanol, and 2.8 mL (for 124 nm sized Si NP) or 3.0 mL (for 148 nm sized Si NP) of aqueous ammonium hydroxide (28–30%) was added to the mixture. The resulting mixture was stirred for 20 h at room temperature. The synthesized Si NPs were centrifuged and then washed with ethanol several times to remove the excess reagents.

Synthesis of bumpy silver nanoshells of different size

AgNSs were synthesized through direct reduction of silver nitrate on thiol-functionalized silica surfaces in the presence of octylamine. Octylamine plays a role not only as a capping ligand, but also as a reducing agent for Ag^+ ions, initiating nucleation of Ag^0 NPs on the surfaces of silica cores and growth to silver shells.[20,21] The Si NPs were dispersed in separate 1 mL ethanol solutions containing 50 μL of MPTS and 10 μL of aqueous ammonium hydroxide (28–30%) for thiol-functionalization. The mixtures were stirred for 6 h at 25 °C, and the resulting MPTS-treated silica NPs were repeatedly centrifuged and dispersed in ethanol. For Si NPs of each size, a different amount of MPTS-treated Si NPs was dispersed in 25 mL ethylene glycol containing 5 mg of PVP, and then 25 mL of an $AgNO_3$ solution (to a final $AgNO_3$ concentration of 3.5 mM) was added to the preparation. The suspension was vigorously mixed to achieve silica dispersion. In the case of the smaller Si NPs (42, 59, 82, and 103 nm), 19.5 μL of ethanolamine was rapidly added into the silica preparation. We also used 41.2 μL of octylamine (each final concentration was 5 mM). The resulting mixtures (AgNSs) were stirred for 1 h at 25 °C, and then centrifuged, and washed with ethanol several times for purification. The amounts of MPTS-treated silica NPs used for each size category of Si NPs are shown in ESI Table S2.†

Raman labelling on AgNSs

The AgNSs (5.0×10^{10} particles) in each size were transferred to the 4-fluorobenzenethiol solutions (2 mM in ethanol). The resulting dispersions were shaken for 1 h at room temperature, and then centrifuged and washed with ethanol several times. In order to avoid the aggregation of AgNSs, 1 mL of PVP (0.025 mM in ethanol) was mixed with AgNSs (5.0×10^{10} particles) bearing Raman labels for 30 min, followed by repeated centrifugation and resuspension in deionized water.

Characterization

After fabrication, AgNSs are optically characterized as shown in Fig. 1. UV-Visible extinction spectra of various sized AgNSs were obtained using an UV-Visible spectrometer (Cary 300, Varian, USA). The sizes, morphologies and homogeneities of the AgNSs were analyzed using a scanning electron microscope (SEM; SUPRA 55VP, Carl Zeiss) and a transmission electron microscope (TEM; JEM1010, JEOL). The SERS spectra of the AgNSs were obtained using a confocal Raman microscope (LabRam 300, JY-Horiba). The Raman scattered light for each AgNS was collected in 180° back-scattering geometry and detected using a spectrometer equipped with a thermoelectrically cooled (−70 °C) charge-coupled device (CCD) detector. SERS signals from the samples in a capillary tube were collected using a ×10 objective lens (NA 0.25) with three different laser lines (532, 660,

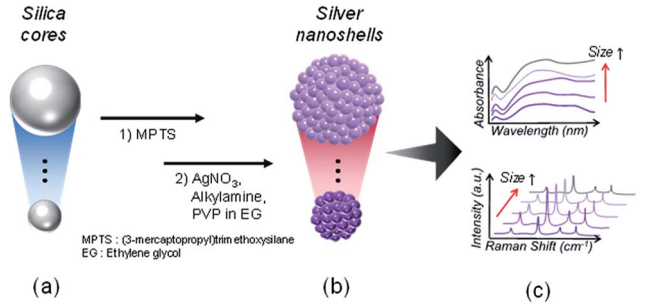

Fig. 1 Schematic illustration for the investigation of the size-dependent optical properties using AgNSs of various sizes. (a) Si NP cores of various sizes, (b) synthesis of AgNSs with tunable sizes using (a). (c) Analysis of the size-dependent optical properties of AgNS and SERS activities.

and 785 nm). The 532 nm laser line from an Nd:YAG laser (Crystal Laser, Reno, NV, USA), the 660 nm laser line from a diode-pumped solid-state laser (Cobolt Flamenco, Sweden), and the 785 nm laser line from a diode-pumped solid-state laser (Crystal Laser, Reno, NV, USA) were used for excitation sources. For single-particle SERS measurement, the samples were dropped on a patterned slide glass, and SERS spectra were measured by point-by-point mapping with a 1 μm step size. The mapping experiments were carried out using a ×100 objective lens (NA 0.90) for three laser lines (532, 660, and 785 nm). After the SERS measurement, SEM images of the same area were obtained for single particle-based analysis. The 20 particles of AgNSs were analyzed for estimation of single-particle SERS activity for each different size of the Si NPs and for each laser line.

Results and discussion

Synthesis and characterization of bumpy silver nanoshells of different sizes

The final size of AgNSs were modulated by controlling the size of the silica cores. AgNS from 170 nm sized Si NP (denoted as AgNS_C170) was successfully fabricated by a previously reported method.[20] However, we found that small core sizes affected the Ag shelling process. When using the same method,[20] AgNS fabricated from 40 nm sized Si NP (denoted as AgNS_C40) formed aggregates to decrease the relatively high surface energies due to the small core sizes (ESI Fig. S1a and b†).[18] For the successful synthesis of smaller AgNSs, the reaction condition needed to be modified to achieve a balance between aggregation (partial shell formation) and over-shelling in the fabrication processes. The proper Ag shelling conditions for maintaining dispersion stabilities of AgNSs were found by using different kinds of alkylamines, such as ethanolamine and propanolamine, instead of octylamine, and by varying the amounts of silica cores, PVP, and $AgNO_3$ (see ESI Fig. S2†). Hence, AgNS_C40 could be fabricated without aggregation, as shown in ESI Fig. S1c.† Note that tuning the amount of Si NPs for the different size Ag shell seemed to be a critical factor for successful AgNS formation. Si NPs in excess of certain ratios easily led to agglomeration. Poor yields with over-shelling of structures were obtained when the amounts of the Si NPs dropped below certain ratios. This result led to reduction in the typical optical properties of Ag shell conferred by the hollow NPs. The UV-Visible-NIR spectra of the AgNS_C170 and AgNS_40 are shown in ESI Fig. S1d.† The AgNS_40 that was obtained by the modified fabrication condition exhibited the common feature of a broad absorption peak spanning the NIR region as shown by AgNS_C170, while the AgNS_C40 prepared by the previous condition exhibited an absorption band near 470 nm caused by an incomplete silver coating.[8]

In order to obtain AgNSs of different sizes, we used Si NP cores of various sizes (59, 82, 103, 124, and 148 nm in average) as starting materials, as shown in Fig. 2a. As mentioned above, the amounts of Si NPs were varied according to the sizes for controlling the reacting surface area of Si NPs, as shown in ESI Table S2.† As a result, we obtained the AgNSs of 119, 152, 165, 186 and 207 nm sizes, respectively, with bumpy morphologies (Fig. 2b and c), and the relative size distributions of AgNSs were 21%, 6.6%, 6.7%, 6.5%, and 3.4% respectively (ESI Table S3†). The monodispersity of AgNSs generally increased with their sizes. The Ag shell thickness was controlled to around ~30 nm for all the AgNSs. The detailed information of the cores, final sizes, and the shell thickness are summarized in ESI Table S3.†

The extinction spectrum of each different AgNS was shown in Fig. 2d. In all cases, the AgNSs exhibited broad extinction features over the almost entire visible range (350–800 nm)

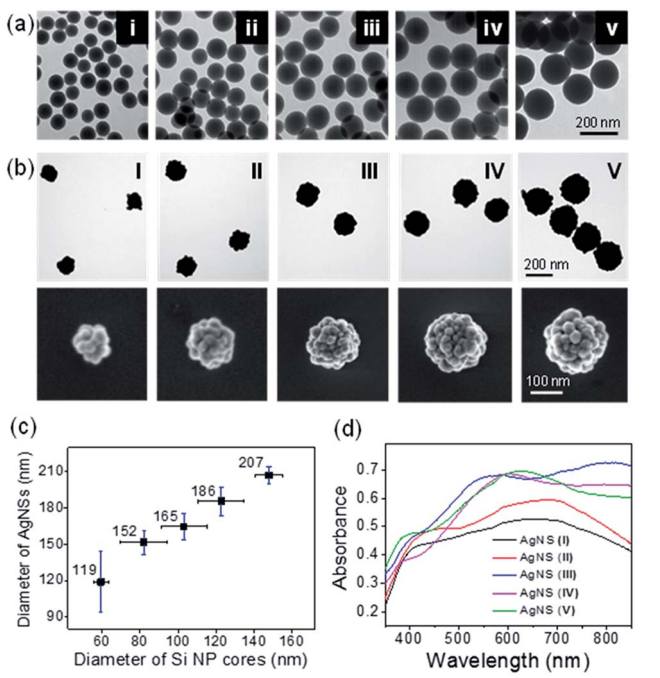

Fig. 2 Synthesis of bumpy silver nanoshells (AgNSs) of various sizes using silica nanoparticles (Si NPs) of various sizes. (a) TEM images of Si NPs with diameters of (i) 59 nm, (ii) 82 nm, (iii) 103 nm, (iv) 124 nm, and (v) 148 nm in average. (b) The TEM (upper panel) and SEM (lower panel) images of the synthesized AgNS of (I) 119 nm, (II) 152 nm, (III) 165 nm, (IV) 186 nm, and (V) 207 nm. Using the Si NPs of (a). (c) Correlation between the diameters of Si NP cores (i)–(v) and those of AgNSs (I)–(V) (mean ± S.D., $n = 20$). (d) The absorption spectra of AgNSs (I)–(V).

regardless of their sizes. It reveals that the size-tuned AgNSs have potentials as effective SERS nanoprobes over the entire visible wavelength range and that the size of AgNSs could be selected for each application. Most of the AgNSs exhibited strong absorption from the visible to the NIR region, while the smaller ones gave slightly decreased absorption at longer wavelengths. It might be attributed to the fact that the excitation cross-sections of larger AgNSs depend on higher-order multiple modes which cause the plasmonic resonance shifts to longer wavelengths and the broadening of bandwidths in addition to dipole absorption.[24]

Roughness parameters according to the size of AgNS

It is well known that roughened noble metal surfaces could contribute to strong SERS enhancements by producing effective SERS active sites with concentrated local electromagnetic fields.[25] In order to relate to the size-dependent SERS enhancement of AgNS with the roughness of AgNS, we need to define the roughness of each different size of the AgNS. AgNS is composed of a Si NP as a core particle and Ag NPs that are assembled on the surface of the silica core, forming a bumpy shell. Because the thickness of Ag NPs formed on a core with a different size was similarly controlled to be *ca.* 30 nm, as shown in ESI Fig. S3,† we could expect that the roughness would increase with a drop in core size.

To quantitatively correlate the roughness of AgNS to its size, we estimated the roughness using a simple model. We defined the roughness as an arithmetic average of deviation heights.[26,27] Fig. 3a illustrates the method for estimating the roughness of AgNS. First, a mean line sphere (MLS) was defined; the sphere of equal volume with single AgNS was termed as MLS. Then, the non-overlapping volume between MLS and AgNS was normalized by the surface of MLS. The roughness (R) of individual AgNS was defined by the following equation:[27,28]

$$R = \frac{1}{Ar}\int\int_{A}^{S} |Z(x,y)|\mathrm{d}x\mathrm{d}y,$$

where A is the surface of MLS, r is the radius (mean curvature) of MLS, and $Z(x, y)$ is deviation height. Therefore, the integral of $|Z(x, y)|$ corresponds to the sum of deviation heights, namely non-overlapping volume between MLS and AgNS. The sum of deviation heights (total volume above/below the MLS) was divided by the surface area of MLS (A) to calculate the arithmetic average of deviation heights. Because curvatures of the substrate (Si NP) also matter in evaluating roughness, normalization of this effect also required. Thus, curvatures of MLS ($1/r$) are reflected in this calculation. The calculated roughness decreased as the size of AgNS became larger (Fig. 3b). The trend of roughness is in good agreement with our assumption that the roughness would increase with a reduction in core size. The detailed method and the calculation results are shown in ESI Fig. S4 and Table S4.†

The size effect of AgNSs on SERS activity

Finally, we explored the SERS activity of the AgNSs depending on the excitation wavelength. Each AgNS was treated with

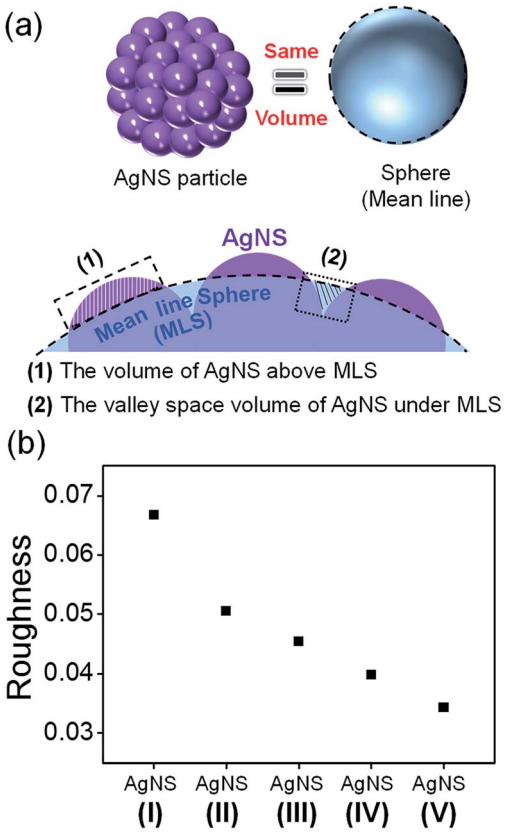

Fig. 3 Roughness of AgNSs (I)–(V). (a) Illustration of modeling for calculation of roughness factors. The boxes with dashed/dotted line represent the volumes of AgNS above/below the mean line sphere. (b) Calculated roughness factors according to the sizes of AgNSs.

4-FBT, which was chemisorbed on the silver shell surfaces. Due to the additional treatment with PVP, 4-FBT labeled AgNSs ($AgNS_{4\text{-FBT}}$) were well dispersed in ethanol without aggregation in solution as shown in ESI Fig. S5.† The Raman spectrum of 4-FBT adsorbed on AgNSs of the same particle concentration in ethanol solution was measured using three different laser line excitations (532, 660 and 785 nm), and normalized with a typical band of ethanol (882 cm^{-1}) (ESI Fig. S6a†). To investigate SERS enhancement factor[29] according to the size of AgNS, the band intensity at 1075 cm^{-1} was normalized with the surface area (ESI Fig. S6b†). The result showed that the SERS activities decreased as the AgNS size increased regardless of laser excitation wavelength, except for the case of the smallest AgNS. The SERS activities of $AgNS_{4\text{-FBT}}$ increased with an increase of the excitation wavelengths from the visible to the NIR region. The result was consistent with the previous report showing that the AgNS is an effective NIR-active substrate.[20,21]

Interestingly, all AgNSs showed the highest SERS enhancement under 785 nm-excitation rather than 660 nm-excitation although AgNSs generally showed very strong plasmonic absorption in the range of 600–700 nm. Many studies have been reported in relation to the correlation between optical plasmon resonance and SERS enhancement. In a simple system, the best excitation was a little blue-shifted with respect to the LSPR

maximum.[30] However, in more complex systems, another typical observation showed that the randomly distributed hot spots present excitation laser lines far away from the LSPR.[31] For a hot spot dominated system, the enhancing properties do not follow the spectral properties of the LSPR demonstrating a separation of LSPR and SERS dispersion. In our previous study, a similar discrepancy between the LSPR maximum and the highest SERS excitation was observed.[20] Such a discrepancy can be understood by the difference of LSPR extinction and SERS:LSPR extinction represents ensemble linear-averaged feature of numerous hot spot sites and other area of nanoparticles while SERS intensity can be contributed dominantly by certain hot spot sites that are optimally resonant with the incident light and stokes Raman scattered light that has always longer wavelength than the incident one. Our DDA results revealed that a highly localized E-field at the tips of the bumpy AgNS surface was shown under the NIR incident light (785 nm), which was 2.6 times larger than the value under visible incident light (532 nm).[20]

To verify more clearly the correlation between the size and the SERS enhancement of AgNS, SERS activities of $AgNS_{4\text{-}FBT}$ were further investigated at single-particle level with three different lasers, as shown in Fig. 4. After the single-particle SERS measurements had been performed by point-by-point mapping on AgNS-dispersed glass slides, the SEM images were obtained and compared with the corresponding SERS intensity maps for verification of the particle locations. For example, a representative SERS intensity map for the 1075 cm^{-1} Raman band of the $AgNS_{4\text{-}FBT}$ (152 nm) was overlaid with the corresponding SEM image (Fig. 4a). Fig. 4b shows a typical SERS spectrum of a single $AgNS_{4\text{-}FBT}$. The SERS enhancement factors (EF) of AgNSs were calculated to be range from 6.4×10^5 to 2.2×10^7 at the three excitation wavelengths (see ESI†). And SERS enhancement of a single AgNS had a similar tendency to SERS activity compared with AgNS in solution and AgNS (152 nm) exhibited the maximum enhancement among the other AgNSs of different sizes (Fig. 4c). This highly sensitive SERS effect could come from the bumpy structure of AgNSs generating strong electric fields regardless of the particle sizes.[20] In addition, the strong SERS activity of the AgNSs indicates that all the AgNSs, regardless of the sizes, could be used for the SERS-based molecular detection with visible to NIR excitation wavelengths.

The relationship between SERS intensities and the roughness factor is shown in Fig. 4d. The SERS activity increased as the roughness factor increased, reaching a maximum at the roughness factor value of 3.51 with AgNS (152 nm). This result clearly shows a correlation between the roughness and the SERS activity, except for the case of the smallest AgNS. This particle was an outlier, probably due to its heterogeneous surface state compared to other NPs of bigger sizes. As shown in the ESI Fig. S7,† the AgNS (119 nm) exhibited a large size variation, partially due to incomplete shell formation and aggregation of NPs. Therefore, the NP gave relatively low SERS activities, although it had the largest roughness.

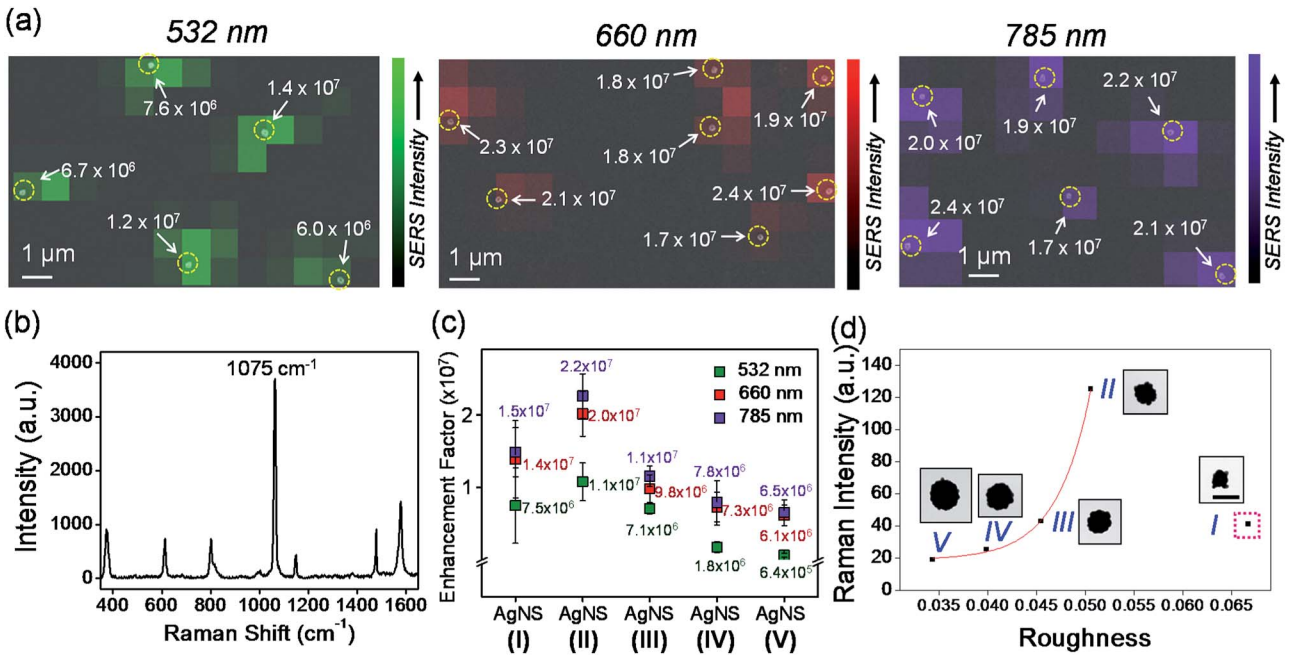

Fig. 4 Single-particle detection of different sized AgNSs. (a) Representative SERS intensity maps of a single AgNS (II) particle with enhancement factor values at 1075 cm^{-1}; the intensity map was overlaid with their corresponding SEM image. Laser powers; 532 nm laser: 1.2 mW, 660 nm laser: 1.6 mW, 785 nm laser: 1.8 mW at sample (b) SERS spectrum obtained from a single particle $AgNS_{4\text{-}FBT}$ (II) on a sliding glass. The spectrum was taken with 532 nm photo-excitation and 2 s acquisition time. (c) Calculated enhancement factors of single AgNSs (I)–(V) based on SERS intensity of 1075 cm^{-1}. (d) Correlation between the roughness and Raman intensity (785 nm laser). The Raman intensity decreased as the roughness of particles (II)–(V) decreased except AgNS (I) in the red dotted box. The red curve exhibits the strong exponential relationship between the roughness of AgNSs (II)–(V) and the SERS intensities. The scale bar is 200 nm.

Our interpretation is that the roughness-dependent SERS activity mainly comes from the different degree of conjunctions among bumps on each surface of the AgNS, termed as hot spots. The hot spots can mostly contribute to the localized electromagnetic mechanism,[32] and consequently, the SERS activity was governed by the roughness. When the size of AgNS was increased, the electromagnetic field at the hot spot was decreased, resulting in a decrease of its SERS activity. Therefore, the size of the AgNS showed a good correlation with the SERS enhancement, which is related to roughness.

Conclusions

In summary, we have analyzed the SERS activities of AgNSs of different sizes and roughness and successfully demonstrated their size-dependent SERS characteristics. The diameters of AgNSs can be finely tuned from ~119 nm to ~207 nm by changing the size of the silica core. All the AgNSs showed strong SERS activities at single-particle levels, and SERS enhancement factors were estimated to range from 6.4×10^5 to 2.2×10^7 at three different laser excitation wavelengths (532, 660 and 785 nm). The SERS activity was increased by increasing their roughness and reducing overall sizes, and the highest SERS signal was observed from a AgNS of 152 nm. Our results can provide the basis to select appropriate AgNSs for specific research purposes.

Conflicts of interest

There are no conflicts to declare.

Acknowledgements

This research was supported by Korea Health Industry Development Institute (KHIDI), funded by the Ministry of Health & Welfare (HI17C1264), and the National Research Foundation (NRF) of Korea, funded by the Ministry of Science, ICT & Future Planning (NRF-2016M2A2A4A03913619).

Notes and references

1 S. Schlücker, *Angew. Chem., Int. Ed.*, 2014, **53**, 4756–4795; S. S. Dasary, A. K. Singh, D. Senapati, H. Yu and P. C. Ray, *J. Am. Chem. Soc.*, 2009, **131**, 13806–13812; W. Smith, *Chem. Soc. Rev.*, 2008, **37**, 955–964.

2 K. Kneipp, Y. Wang, H. Kneipp, L. T. Perelman, I. Itzkan, R. R. Dasari and M. S. Feld, *Phys. Rev. Lett.*, 1997, **78**, 1667.

3 G. C. Schatz, M. A. Young and R. P. Van Duyne, in *Surface-enhanced Raman scattering*, Springer, 2006, pp. 19–45; Z.-Q. Tian and B. Ren, *Annu. Rev. Phys. Chem.*, 2004, **55**, 197–229.

4 S. Nie and S. R. Emory, *Science*, 1997, **275**, 1102–1106.

5 S. Schlücker, *ChemPhysChem*, 2009, **10**, 1344–1354.

6 N. T. Thanh, N. Maclean and S. Mahiddine, *Chem. Rev.*, 2014, **114**, 7610–7630.

7 B. Küstner, M. Gellner, M. Schütz, F. Schöppler, A. Marx, P. Ströbel, P. Adam, C. Schmuck and S. Schlücker, *Angew. Chem., Int. Ed.*, 2009, **48**, 1950–1953; C. E. Talley, J. B. Jackson, C. Oubre, N. K. Grady, C. W. Hollars, S. M. Lane, T. R. Huser, P. Nordlander and N. J. Halas, *Nano Lett.*, 2005, **5**, 1569–1574.

8 H. Kang, J. Yim, S. Jeong, J.-K. Yang, S. Kyeong, S.-J. Jeon, J. Kim, K. D. Eom, H. Lee and H.-I. Kim, *ACS Appl. Mater. Interfaces*, 2013, **5**, 12804–12810.

9 A. M. Schwartzberg, T. Y. Olson, C. E. Talley and J. Z. Zhang, *J. Phys. Chem. B*, 2006, **110**, 19935–19944; V. Vongsavat, B. M. Vittur, W. W. Bryan, J. H. Kim and T. R. Lee, *ACS Appl. Mater. Interfaces*, 2011, **3**, 3616–3624; H. Chon, C. Lim, S. M. Ha, Y. Ahn, E. K. Lee, S. I. Chang, G. H. Seong and J. Choo, *Anal. Chem.*, 2010, **82**, 5290–5295.

10 Y. Zhang, J. Qian, D. Wang, Y. Wang and S. He, *Angew. Chem., Int. Ed.*, 2013, **52**, 1148–1151; M. F. Kircher, A. de la Zerda, J. V. Jokerst, C. L. Zavaleta, P. J. Kempen, E. Mittra, K. Pitter, R. Huang, C. Campos, F. Habte, R. Sinclair, C. W. Brennan, I. K. Mellinghoff, E. C. Holland and S. S. Gambhir, *Nat. Med.*, 2012, **18**, 829–834; J. V. Jokerst, A. J. Cole, D. Van de Sompel and S. S. Gambhir, *ACS Nano*, 2012, **6**, 10366–10377.

11 H. Yuan, A. M. Fales, C. G. Khoury, J. Liu and T. Vo-Dinh, *J. Raman Spectrosc.*, 2013, **44**, 234–239; L. Rodríguez-Lorenzo, Z. Krpetic, S. Barbosa, R. A. Álvarez-Puebla, L. M. Liz-Marzán, I. A. Prior and M. Brust, *Integr. Biol.*, 2011, **3**, 922–926; H. Yuan, Y. Liu, A. M. Fales, Y. L. Li, J. Liu and T. Vo-Dinh, *Anal. Chem.*, 2013, **85**, 208–212.

12 S. J. Oldenburg, G. D. Hale, J. B. Jackson and N. J. Halas, *Appl. Phys. Lett.*, 1999, **75**, 1063–1065.

13 J. Jackson and N. Halas, *J. Phys. Chem. B*, 2001, **105**, 2743–2746; S. Tang, Y. Tang, S. Zhu, H. Lu and X. Meng, *J. Solid State Chem.*, 2007, **180**, 2871–2876.

14 N. Halas, *MRS Bull.*, 2005, **30**, 362–367.

15 E. Prodan and P. Nordlander, *Nano Lett.*, 2003, **3**, 543–547.

16 J. B. Jackson and N. J. Halas, *Proc. Natl. Acad. Sci. U. S. A.*, 2004, **101**, 17930–17935.

17 K.-T. Yong, Y. Sahoo, M. T. Swihart and P. N. Prasad, *Colloids Surf., A*, 2006, **290**, 89–105; R. A. Alvarez-Puebla, D. J. Ross, G.-A. Nazri and R. F. Aroca, *Langmuir*, 2005, **21**, 10504–10508; S. Westcott, J. Jackson, C. Radloff and N. Halas, *Phys. Rev. B: Condens. Matter Mater. Phys.*, 2002, **66**, 155431; S. J. Oldenburg, S. L. Westcott, R. D. Averitt and N. J. Halas, *J. Chem. Phys.*, 1999, **111**, 4729–4735.

18 M. Kobayashi, F. Juillerat, P. Galletto, P. Bowen and M. Borkovec, *Langmuir*, 2005, **21**, 5761–5769.

19 H. Chang, H. Kang, J. K. Yang, A. Jo, H. Y. Lee, Y. S. Lee and D. H. Jeong, *ACS Appl. Mater. Interfaces*, 2014, **6**, 11859–11863; D. Yim, H. Kang, S. J. Jeon, H. I. Kim, J. K. Yang, T. W. Kang, S. Lee, J. Choo, Y. S. Lee, J. W. Kim and J. H. Kim, *Analyst*, 2015, **140**, 3362–3367.

20 H. Kang, J.-K. Yang, M. S. Noh, A. Jo, S. Jeong, M. Lee, S. Lee, H. Chang, H. Lee and S.-J. Jeon, *J. Mater. Chem. B*, 2014, **2**, 4415–4421.

21 J.-K. Yang, H. Kang, H. Lee, A. Jo, S. Jeong, S.-J. Jeon, H.-I. Kim, H.-Y. Lee, D. H. Jeong, J.-H. Kim and Y.-S. Lee, *ACS Appl. Mater. Interfaces*, 2014, **6**, 12541–12549.

22 R. P. Bagwe, C. Yang, L. R. Hilliard and W. Tan, *Langmuir*, 2004, **20**, 8336–8342; L. Yao, G. Xu, W. Dou and Y. Bai, *Colloids Surf., A*, 2008, **316**, 8–14.

23 W. Stöber, A. Fink and E. Bohn, *J. Colloid Interface Sci.*, 1968, **26**, 62–69.

24 S. Link and M. A. El-Sayed, *J. Phys. Chem. B*, 1999, **103**, 4212–4217; P. P. Fang, J. F. Li, Z. L. Yang, L. M. Li, B. Ren and Z. Q. Tian, *J. Raman Spectrosc.*, 2008, **39**, 1679–1687.

25 M. S. Schmidt, J. Hubner and A. Boisen, *Adv. Mater.*, 2012, **24**, OP11–OP18; Y.-L. Deng and Y.-J. Juang, *Biosens. Bioelectron.*, 2014, **53**, 37–42; M. Baibarac, M. Cochet, M. Łapkowski, L. Mihut, S. Lefrant and I. Baltog, *Synth. Met.*, 1998, **96**, 63–70; J. I. Gersten, *J. Chem. Phys.*, 1980, **72**, 5779–5780.

26 E. Gadelmawla, M. Koura, T. Maksoud, I. Elewa and H. Soliman, *J. Mater. Process. Technol.*, 2002, **123**, 133–145.

27 J. Rosales-Leal, M. Rodríguez-Valverde, G. Mazzaglia, P. Ramon-Torregrosa, L. Diaz-Rodriguez, O. Garcia-Martinez, M. Vallecillo-Capilla, C. Ruiz and M. Cabrerizo-Vilchez, *Colloids Surf., A*, 2010, **365**, 222–229.

28 J. Sauri, J. M. Sune-Negre, J. Diaz-Marcos, J. Vilana, D. Millan, J. R. Tico, M. Minarro, P. Perez-Lozano and E. Garcia-Montoya, *Int. J. Pharm.*, 2015, **478**, 328–340.

29 B. H. Jun, G. Kim, J. Baek, H. Kang, T. Kim, T. Hyeon, D. H. Jeong and Y. S. Lee, *Phys. Chem. Chem. Phys.*, 2011, **13**, 7298–7303.

30 A. D. McFarland, M. A. Young, J. A. Dieringer and R. P. Van Duyne, *J. Phys. Chem. B*, 2005, **109**, 11279–11285.

31 S. Abalde-Cela, S. Ho, B. Rodriguez-Gonzalez, M. A. Correa-Duarte, R. A. Alvarez-Puebla, L. M. Liz-Marzan and N. A. Kotov, *Angew. Chem., Int. Ed.*, 2009, **48**, 5326–5329; S. L. Kleinman, B. Sharma, M. G. Blaber, A. I. Henry, N. Valley, R. G. Freeman, M. J. Natan, G. C. Schatz and R. P. Van Duyne, *J. Am. Chem. Soc.*, 2013, **135**, 301–308.

32 H. Ko, S. Singamaneni and V. V. Tsukruk, *Small*, 2008, **4**, 1576–1599; L. Li, T. Hutter, U. Steiner and S. Mahajan, *Analyst*, 2013, **138**, 4574–4578; H. Liu, L. Zhang, X. Lang, Y. Yamaguchi, H. Iwasaki, Y. Inouye, Q. Xue and M. Chen, *Sci. Rep.*, 2011, **1**, 112.